Available online at www.sciencedirect.com
SCIENCE DIRECT®
Journal of Organometallic Chemistry 683 (2003) 341–353
Journal of Organometallic Chemistry
www.elsevier.com/locate/jorganchem

Carbon-rich organometallic materials derived from 4-ethynylphenylferrocene

Wai-Yeung Wong [a,*], Ka-Yan Ho [a], Sze-Ling Ho [a], Zhenyang Lin [b]

[a] Department of Chemistry, Hong Kong Baptist University, Waterloo Road, Kowloon Tong, Hong Kong, China
[b] Department of Chemistry, Hong Kong University of Science and Technology, Clearwater Bay, Hong Kong, China

Received 7 May 2003

Abstract

Using 4-ethynylphenylferrocene (**1**) as the building block, a new series of rigid-rod alkynylferrocenyl precursors consisting of fluoren-9-one unit, 2-bromo-7-(4-ferrocenylphenylethynyl)fluoren-9-one (**2a**), 2,7-bis(4-ferrocenylphenylethynyl)fluoren-9-one (**2b**), 2-trimethylsilylethynyl-7-(4-ferrocenylphenylethynyl)fluoren-9-one (**3**) and 2-ethynyl-7-(4-ferrocenylphenylethynyl)fluoren-9-one (**4**) have been prepared in moderate to good yields. The acetylene complex **4** is a useful precursor for the synthesis of well-defined carbon-rich ferrocenyl heterometallic complexes, *trans*-[(η^5-C_5H_5)Fe(η^5-C_5H_4)C_6H_4C≡CRC≡CPt(PEt_3)$_2$Ph] (**5**), *trans*-[(η^5-C_5H_5)Fe(η^5-C_5H_4)C_6H_4C≡CRC≡CPt(PBu_3)$_2$C≡CRC ≡ CC_6H_4(η^5-C_5H_4)Fe(η^5-C_5H_5)] (**6**), *trans*-[(η^5-C_5H_5)Fe(η^5-C_5H_4)C_6H_4C≡CRC≡CM(dppm)$_2$Cl] (M = Ru (**7**), Os (**8**)) (R = fluoren-9-one-2,7-diyl). All new complexes have been characterized by FTIR, NMR and UV–Vis spectroscopies and fast atom bombardment mass spectrometry (FABMS). The molecular structures of **1**, **2a**, **4**, **6** and **8** have been determined by single-crystal X-ray studies where an iron–iron through-space distance of nanosized dimension (ca. 42 Å) is observed in the trimetallic molecular rod **6**. The electronic absorption, luminescence and electrochemical properties of these carbon-rich molecules were investigated and the data were correlated with the theoretical results obtained by the method of density functional theory.
© 2003 Elsevier B.V. All rights reserved.

Keywords: Alkynyl complexes; Ferrocene; Fluorenone; Platinum; Osmium

1. Introduction

Carbon-rich organometallic compounds containing rigid, π-conjugated fragments continue to constitute an important research frontier because of their wide applications in many areas of materials science [1]. It has been well documented that molecular wires comprising mixed-valence bimetallic units or remote redox-active organometallic groups linked by all-carbon chains could be exploited in molecular electronics, optoelectronic and chemical-sensing devices [2]. Molecular wires with through-space metal-to-metal distance of up to 40 Å and an effective conjugation pathway of up to 50 Å are also known [3]. Molecules of this type would be useful models for conducting polymers that have metal centers incorporated into their backbone. Although the first report of the mixed-valence ion of diferrocenylacetylene was reported as early as 1974 [4], interest in metal-capped linear polycarbon chains as models for materially useful compounds is still very intense and much research efforts have been devoted to the molecular design of ferrocene-derived homo- and heterometallic molecular scaffolds connected by a wide variety of organic aromatic and heteroaromatic spacers as well as oligoacetylenic units [5–7]. The introduction of a metallocene unit into "rigid-rod" one-dimensional oligomers and polymers may lead to a range of properties (e.g. redox, optical, electrical and catalytic properties) that differ from those of conventional organic polymers [5,6].

Our research group has recently initiated a program to develop rational synthetic routes to some well-defined oligoacetylenic ferrocenyl complexes with bridging units such as oligothiophenes and functionalized 2,7-fluorenes

* Corresponding author. Tel.: +852-3411-7074; fax: +852-3411-7348.
E-mail address: rwywong@hkbu.edu.hk (W.-Y. Wong).

0022-328X/03/$ - see front matter © 2003 Elsevier B.V. All rights reserved.
doi:10.1016/S0022-328X(03)00706-X

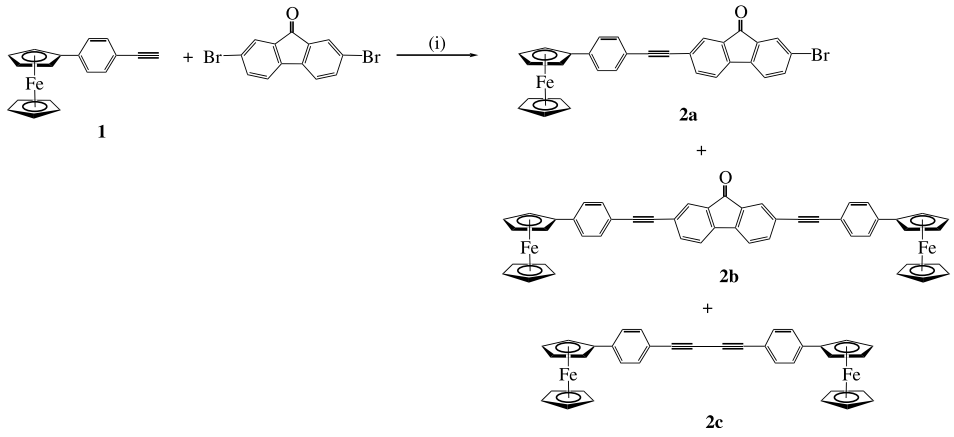

Scheme 1. (i) $Pd(OAc)_2$, CuI, PPh_3, $^iPr_2NH$.

by a series of controlled coupling sequences based on ethynylferrocene [7]. Our interest in the employment of these organic linkers in molecular design stems from the fact that materials derived from them usually possess intriguing luminescent and physical properties [8]. Alkynyl ligands can offer synthetic versatility and structural rigidity and have great potentials to allow electronic communication between redox-active terminal end groups through delocalized bonds [6]. X-ray crystallographic studies of several of these molecules in the solid state allow an iron–iron through-space separation of up to ca. 34 Å to be estimated [7b,7c]. In the quest for new alkynylferrocene-based materials, it seemed an attractive goal to us to develop new molecular architectures based on the more extended congener, 4-ethynylphenylferrocene (**1**), and such a study should represent an interesting extension to the chemistry of related systems. We report in this paper the synthesis, characterization as well as photophysical, redox and structural properties of a new series of carbon-rich organometallic oligoacetylide complexes using **1** as the building unit, and molecular orbital calculations of these molecules, at the B3LYP level of density functional theory, have been carried out in order to compare the results with the experimental data.

2. Results and discussion

2.1. Synthesis

Following an expansion of our previously reported ferrocenyl metal-acetylide systems [7], the Sonogashira coupling reaction of 4-ethynylphenylferrocene (**1**) with an excess of 2,7-dibromofluoren-9-one gave 2-bromo-7-(4-ferrocenylphenylethynyl)fluoren-9-one (**2a**) and 2,7-bis(4-ferrocenylphenylethynyl)fluoren-9-one (**2b**) as the major products, accompanied by the formation of 1,4-bis(4-ferrocenylphenyl)butadiyne (**2c**) obtained via simultaneous oxidative coupling of **1** in the presence of a trace amount of atmospheric O_2 (Scheme 1). We have been able to minimize the yield of the homocoupling product **2c** ($< 5\%$) under almost anaerobic conditions. After conversion of the mono-bromo species **2a** to 2-trimethylsilylethynyl-7-(4-ferrocenylphenylethynyl)fluoren-9-one (**3**) using the established method [7], desilylation of **3** with K_2CO_3 in MeOH readily afforded 2-ethynyl-7-(4-ferrocenylphenylethynyl)fluoren-9-one (**4**) that was used for the build-up of the following multimetallic systems. Scheme 2 outlines the synthetic routes to the various bi- and trimetallic complexes in our study. The classical dehydrohalogenation reactions between **3** and *trans*-$[Pt(PEt_3)_2(Ph)Cl]$ or *trans*-$[Pt(PBu_3)_2Cl_2]$ led to new platinum(II) alkynyl complexes *trans*-$[(\eta^5\text{-}C_5H_5)Fe(\eta^5\text{-}C_5H_4)C_6H_4C{\equiv}CRC{\equiv}CPt(PEt_3)_2Ph]$ (**5**) and *trans*-$[(\eta^5\text{-}C_5H_5)Fe(\eta^5\text{-}C_5H_4)C_6H_4C{\equiv}CRC{\equiv}CPt(PBu_3)_2C{\equiv}CRC{\equiv}CC_6H_4(\eta^5\text{-}C_5H_4)Fe(\eta^5\text{-}C_5H_5)]$ (**6**) (R = fluoren-9-one-2,7-diyl) in good yields and these products were purified by preparative TLC on silica [7,8c,8d,8e,8f]. New σ-acetylide complexes of Group 8 metals *trans*-$[(\eta^5\text{-}C_5H_5)Fe(\eta^5\text{-}C_5H_4)C_6H_4C{\equiv}CRC{\equiv}CM(dppm)_2Cl]$ (M = Ru (**7**), Os (**8**)) (R = fluoren-9-one-2,7-diyl) were made by reacting *cis*-$[M(dppm)_2Cl_2]$ (M = Ru, Os) with $NaPF_6$ to give first the vinylidene intermediates which can be deprotonated by DBU to furnish the desired compounds [9] and pure samples of **7** and **8** were obtained in satisfactory yields after passage of the crude products through a short alumina column. All new complexes exhibit good air stability and solubility in common organic solvents. The proposed formulations of the new complexes were all in accord with their analytical and spectroscopic (FTIR, NMR and MS) data and the molecular structures of representative compounds have been determined unequivocally by single-crystal X-ray analyses.

2.2. Spectroscopic properties

All new compounds display weak to moderate ν(C≡C) absorptions in their IR spectra and all fluorenone-

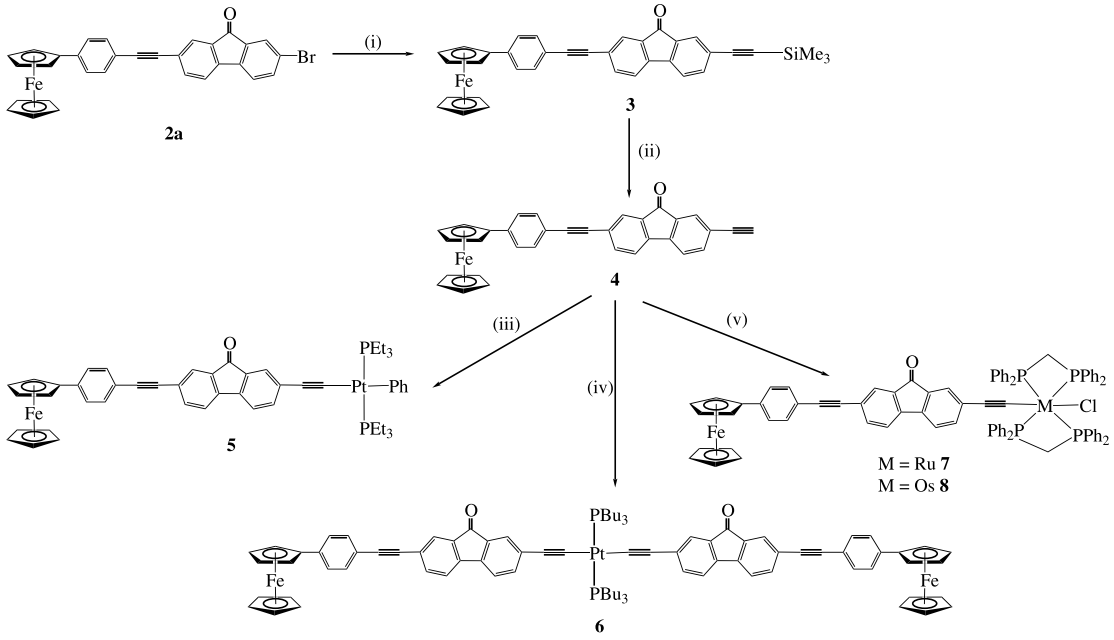

Scheme 2. (i) Trimethylsilylacetylene, $Pd(OAc)_2$, CuI, PPh_3, $^iPr_2NH$; (ii) K_2CO_3, MeOH; (iii) *trans*-$[Pt(PEt_3)_2(Ph)Cl]$, CuI, $^iPr_2NH$; (iv) trans-$[Pt(PBu_3)_2Cl_2]$ (0.5 equiv.), CuI, $^iPr_2NH$; (v) *cis*-$[M(dppm)_2Cl_2]$ (M = Ru, Os), $NaPF_6$, DBU.

containing compounds show ν(C≡O) vibrations at about 1720 cm^{-1}. The C≡*C*–*H* stretching band also occurs at 3302 cm^{-1} for **4**. For **3**–**6**, two ν(C≡C) bands are observed and those at the higher frequencies absorb at similar energies in each case and compare well with the value (2213 cm^{-1}) found in **2b**. The lower frequency ν(C≡C) band appears lower in energy for **5** and **6** than that found in the uncoordinated precursor **4**, in line with the back-bonding effect of the Pt(II) center to the acetylide unit. Proton NMR signals typical of mono-substituted ferrocene and aromatic fluorenone were all apparent in the new complexes. The simplicity of the IR (two ν(C≡C) stretching frequencies) and $^{31}P\{^1H\}$-NMR (singlet, with associated Pt satellites) data indicates the presence of symmetry around the platinum center in **6**. The observation of the room-temperature ^{31}P-NMR signal as a sharp singlet for each of **5**–**8** confirms a *trans* configuration of the bound phosphine ligands at the transition metals. The FABMS and elemental analytical data further support the formulae and composition of these compounds.

2.3. Electronic absorption and luminescence spectra and electrochemistry

Table 1 collects the absorption spectral data of our new complexes recorded in CH_2Cl_2. For the ferrocenyl precursors **2**–**4**, each of them essentially displays three main structureless absorption bands between 250 and 400 nm originating from π–π* electronic transitions of the associated organic groups [7]. The broad low-energy features beyond 400 nm account for the orange colors of these ferrocenyl compounds. Introduction of the platinum(II) segment to **4** causes bathochromic shifts in the lowest energy bands in **5** and **6**, suggesting an enhancement in the extent of π-delocalization through the platinum centers. A red-shift of about 30 nm is observed from **4** to **5** and **6** and these results demonstrate that the conjugation effect is more pronounced in **5** and **6** than in similar compounds obtained from ethynylferrocene [7c]. The electronic spectra of **7** and **8** are characterized by the featureless π–π* transition bands of the alkynylferrocenyl chromophores in the near-UV region accompanied by a broader band at 560 and 598 nm for **7** and **8**, respectively. We note that those transitions in the visible range appear at longer wavelengths for **8** than in the ruthenium counterpart **7**. Because of the significant contribution from the Group 8 metal d-orbitals to the HOMOs in these complexes, we consider that the lowest energy band may be metal-to-ligand charge transfer in nature (vide infra).

All these fluorenone-containing complexes are luminescent in CH_2Cl_2 solutions at room temperature (Table 1) and the emission peaks appear in the range 505–598 nm in the visible region. The luminescence spectra are virtually invariant of the excitation wavelength used. Due to their similar structured peak pattern, we consider that these emission features should have the same origin in each case. By analogy with 2,7-diethynylfluoren-9-one which emits at 531 nm in CH_2Cl_2 [8g], these luminescence bands probably arise from ligand-dominating emissive states and can be assigned to the intraligand π–π* transitions. Comparison of the emission spectra of **4** and the platinum complexes (**5** and **6**)

Table 1
Photophysical and redox data for new complexes in CH_2Cl_2

Complex	λ_{max} (nm) [a]	λ_{em} (nm) [b]	$E_{1/2}$ (V) [c]
2a	279 (1.6), 306 (1.6), 349 (1.4), 457 (0.2)	536	0.07 (92), −1.56 [d]
2b	257 (0.6), 304 (0.4), 348 (0.4), 451 (0.3), 490 (0.2)	598	0.06 (86), −1.58 [d]
2c	258 (0.5), 336 (0.7), 449 (0.1)	–	0.04 (180)
3	286 (2.3), 311 (2.0), 357 (1.9), 457 (0.3)	526	0.09 (97), −1.57 [d]
4	240 (3.5), 283 (6.7), 309 (6.2), 354 (5.5), 454 (0.8)	524	0.10 (96), −1.59 [d]
5	263sh (3.8), 304 (5.3), 330 (3.7), 338 (3.2), 370 (4.6), 488 (0.5)	544	0.79 [d], 0.07 (107)
6	262 (4.9), 305 (7.5), 378 (10.9), 485 (1.5)	545	0.82 [d], 0.06 (158)
7	268 (3.0), 320 (1.7), 405 (1.3), 560 (0.2)	524	0.97 [d], 0.08 (100)
8	302 (3.0), 421 (1.9), 598 (0.4)	505	0.95 [d], 0.07 (107), −0.11 [d]

[a] Extinction coefficients ($\varepsilon \times 10^{-4}$ dm^3 mol^{-1} cm^{-1}) are shown in parentheses.
[b] Excitation wavelength = 330 nm.
[c] Scan rate = 100 mV s^{-1}, half-wave potential values $E_{1/2} = (E_{pa} + E_{pc})/2$ for reversible ferrocenyl oxidation, $\Delta E_p = E_{pa} - E_{pc}$ (in mV) for reversible waves are given in parentheses, where E_{pa} and E_{pc} are the anodic and cathodic peak potentials, respectively.
[d] Irreversible wave.

reveals a red-shift in the emission maxima which also corresponds to the bathochromic shift observed in their absorption spectra.

The electrochemical behavior of our complexes was studied by cyclic voltammetry in CH_2Cl_2 at room temperature and the redox data are listed in Table 1. In each case, the complex is characterized by one quasi-reversible oxidation wave due to the ferrocenyl electrophore that is present. An anodic shift of the ferrocene–ferrocenium couple relative to the ferrocene standard is caused by the unsaturation of the alkynyl units which makes the removal of electrons more difficult than pure ferrocene. Each of the complexes **2b** and **2c** displays only a single two-electron oxidation for the two ferrocenyl groups, indicating no detectable electrocommunication between them. When the conjugation is extended from **4** to **5**–**8** after adding an organometallic segment, only a slight negative shift in $E_{1/2}$ values is observed. Electrochemical studies on the mixed-metal complex **6** indicate that there is no ferrocene–ferrocene interaction through the alkynyl-platinum bridge and it only undergoes a single-step two-electron oxidation involving the concomitant oxidation of the two ferrocenyl subunits at a scan rate of 100 mV s^{-1}. Non-interacting diferrocenyl molecules have been reported in some conjugated organometallic systems [7,10]. Fluorenone-based reduction waves which span the narrow range of −1.56 to −1.59 V are also observed for **2a**, **2b**, **3** and **4**, but they are absent in the heterometallic complexes **5**–**8**. Similar phenomenon has been observed for related compounds derived from ethynylferrocene [7c]. For **5** and **6**, another redox event was detected at higher positive potentials which can be attributed to the irreversible oxidation of the platinum moiety [Pt(II) → Pt(III)]. The potential peak at −0.11 V is most likely to be due to the oxidation of Os(II) core in **8**.

2.4. Crystal structure analyses

The molecular structures of complexes **1**, **2a**, **2c**, **4**, **6** and **8**, as shown by X-ray crystallography, are depicted in Figs. 1–6, respectively. Important bond parameters along with selected dihedral angles are tabulated in Tables 2–7. For **1**, each molecule consists of a ferrocene unit and an acetylene group (C(17)–C(18) = 1.174(3) Å) appended to the phenylene ring in the 1,4-positions. The structure of **2c** possesses a 1,3-butadiyne linear chain with two ferrocenyl substituents in positions 1 and 4 of the chain. Each ferrocenyl moiety lies on opposite sides of the mean plane of the chain and C_5H_4 rings, with a symmetry center at the mid-point of the C(18)–C(18A) bond that coincides with the crystallographic center of symmetry. The C(17)–C(18) (1.184(8) Å) and C(18)–C(18A) (1.391(14) Å) distances are of the order of those observed in 1,4-diferrocenyl-1,3-butadiyne (1.198(4) and 1.373(3) Å, respectively) [11] and 1,12-bis(ferrocenyl)-1,3,5,7,9,11-dodecahexane (1.196(9)–1.224(10) and 1.347(11)–1.404(16) Å) [6c]. Figs. 2 and 4 show that one 4-ferrocenylphenyl unit is attached to one end of 2-bromo-7-ethynylfluoren-9-one and 2,7-diethynylfluoren-9-one, respectively, for **2a** and **4**. The acetylide bonds show normal lengths of 1.161(4)–1.199(3) Å.

For **6**, the crystal structure shows a diferrocenyl end-capped species in which two deprotonated forms of **4** are covalently bonded to the central $Pt(PBu_3)_2$ unit in a *trans* geometry to afford a one-dimensional molecular rod of defined length and the through-space separation between Fe(1) and Fe(2) is estimated to be 42 Å in the solid state, which is larger than the value of 34 Å found in the related complex constructed from ethynylferrocene. Hence, extension of the dimensions of these metal-capped molecules from molecular scale to nanoscale becomes viable based on this synthetic strategy. The corresponding mean Fe–Pt distance is ca. 21 Å. The

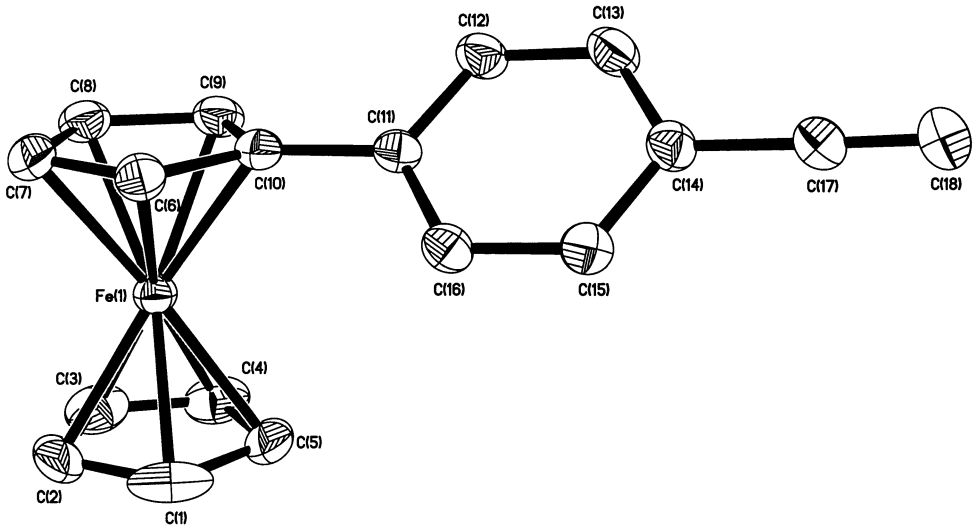

Fig. 1. A perspective view of **1**, showing the atomic labelling scheme. Thermal ellipsoids were drawn at the 25% probability level and hydrogen atoms are omitted for clarity.

platinum center adopts a square-planar geometry and the average Pt–P distance is 2.277(3) Å. The alkynyl bond lengths span the narrow range 1.180(10)–1.206(11) Å, which are comparable to those found in other analogous complexes [7]. The nearly linear bond angles around the alkyne units in **6** conform to the rigid and straight-chain nature of the molecule.

The heterometallic complex **8** has the *trans*-$[Os(dppm)_2Cl]$ fragment bonded to the terminal alkyne unit of 2-ethynyl-7-(4-ferrocenylphenylethynyl)fluoren-9-one where the Os–Cl vector is *trans* to the alkynyl ligand (Cl(1)–Os(1)–C(33) = 174.38(13)°). The coordination at the osmium(II) center is distorted octahedral with the mean Os–P distance of 2.3528(16) Å, which compare well with the structural features observed in other structurally characterized osmium mono-chloro acetylide complexes such as *trans*-$[(\eta^5\text{-}C_5H_5)Fe(\eta^5\text{-}C_5H_4)C{\equiv}COs(dppm)_2Cl]$ [9a] and *trans*-$[(dppm)_2ClOsC{\equiv}CSiC{\equiv}CH]$ [9e]. The alkynyl bond lengths are typical at 1.199(8)–1.207(6) Å.

In each of these alkynylferrocenyl complexes, the cyclopentadienyl rings of the ferrocenyl group are essentially planar and exhibit an eclipsed conformation with deviation angles spanning a narrow range of ca. 0.9–6.8°. Variation of the end groups does not have a great influence on the bond parameters of the ferrocene and fluorenone units. Moreover, all the fluorenonediyl ring systems are planar and the structural parameters within the ring are normal. There are also no short intermolecular contacts and π-stacking of fluorenone units in all these crystal lattices.

2.5. Molecular orbital calculations

To examine the electronic structures and gain a deeper insight into the nature of the frontier molecular orbitals of these carbon-rich organometallic molecules, we have carried out molecular orbital calculations at the B3LYP level of density functional theory (DFT) for complexes **6** and **8** based on their experimental geometries obtained from the X-ray data [12], and the results

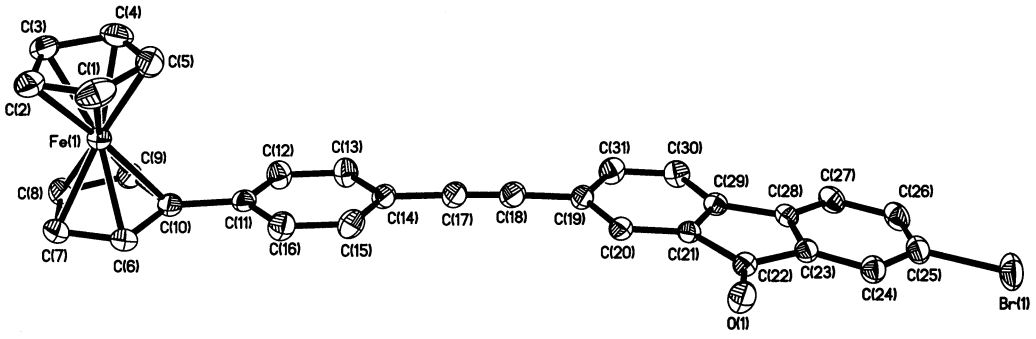

Fig. 2. A perspective view of **2a**, showing the atomic labelling scheme. Thermal ellipsoids were drawn at the 25% probability level and hydrogen atoms are omitted for clarity.

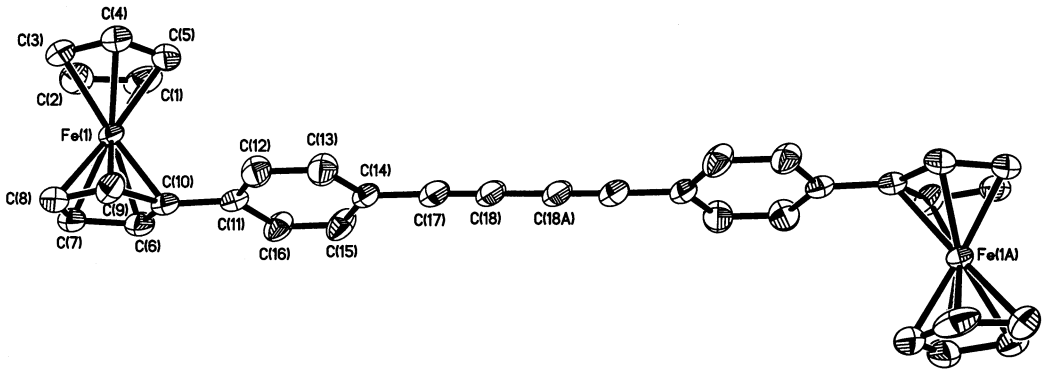

Fig. 3. A perspective view of one molecule of **2c**, showing the atomic labelling scheme. Thermal ellipsoids were drawn at the 25% probability level and hydrogen atoms are omitted for clarity.

are compared to those of **4**. Fig. 7 shows the contour plots [13] of the orbitals in the HOMO–LUMO region for **4**. We found that the three HOMOs for **4** correspond to those derived from the mixing of the highest occupied orbitals of the conjugated organic structural unit and the two Fe(d_δ)-orbitals. The δ-type is defined by viewing the orbitals along the Ct–Fe–Ct axes (Ct: the center of each cyclopentadienyl ligand). When the Ct–Fe–Ct axis is defined as the z-axis, the two d_δ-orbitals correspond to the d_{xy} and $d_{x^2-y^2}$ orbitals. The LUMOs for **4** correspond to the π* orbital in the structural unit having a carbonyl group. Carbonyl groups normally have lower π* orbitals because of the electronegative oxygen atom.

An orbital correlation diagram shown in Fig. 7 is used to illustrate the change in the orbital patterns in **6** and **8** upon incorporation of different metal groups to **4**. The frontier orbitals of **6** are derived from the orbital combinations of the two ferrocenyl-containing alkynyl ligands. The two HOMOs are contributed from the highest occupied π-orbitals of the two ligands whereas the two LUMOs arise from the lowest unoccupied π*-orbitals of the organic portion in the two ligands. The two HOMOs of **8** are derived from the mixing of the Os metal d-orbitals (i.e. d_{xz} and d_{yz} when the Os–Cl bond direction is defined as the z-axis) and π-orbitals of the Os-bonded C≡C unit. The LUMOs correspond to the lowest π*-orbitals of the carbonyl-containing conjugate structural moiety. Because of π-donating properties of the chloride, there are π*-antibonding characters between Os and Cl in the two HOMOs. Therefore, the absorption band corresponding to the HOMO–LUMO transition probably has the MLCT character and the calculated HOMO–LUMO gap (2.69 eV) for **8** is considerably smaller than that for **4** (3.03 eV). The three HOMOs in **4** correspond to the 3rd to 5th HOMOs in **8**. Likewise, the smaller HOMO–LUMO gap for **6** (3.01 eV) in comparison to **4** can be related to their observed UV–Vis data which indicates the possibility of π-conjugation through the platinum unit.

3. Concluding remarks

This report describes the successful use of 4-ethynylphenylferrocene as the synthon to afford a new family of luminescent carbon-rich heterometallic complexes in satisfactory yields. The properties of these compounds were completely elucidated by spectroscopic, electrochemical and X-ray structural techniques. Linear chain growth in two directions around the central platinum moiety was demonstrated in the trimetallic compound **6** by platinum–alkyne bond formation but its cyclic voltammogram shows only one two-electron ferrocenyl redox process, indicating that there is no detectable electrocommunication between the terminal ferrocenyl groups through the carbon-rich links. The two iron(II)

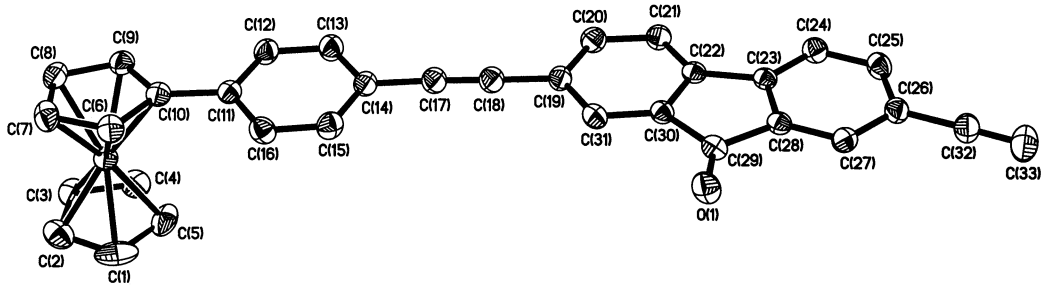

Fig. 4. A perspective view of **4**, showing the atomic labelling scheme. Thermal ellipsoids were drawn at the 25% probability level and hydrogen atoms are omitted for clarity.

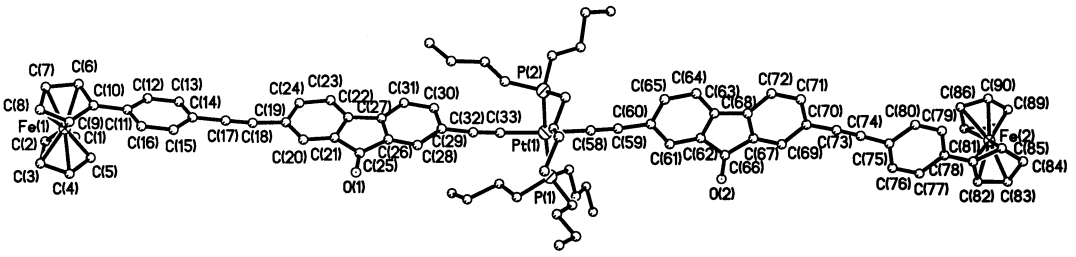

Fig. 5. A perspective view of **6**, showing the atomic labelling scheme. Hydrogen atoms and labels on the butyl groups are omitted for clarity.

centers at the ferrocenyl termini of **6** show a very long through-space distance of ca. 42 Å and we have been able to extend the dimensions of these rigid-rod-like complexes from the molecular scale to nanoscale which is essential for the further development of nanoscale molecular wires and related nanomaterials. Our experimental results show that delocalization of π electrons continues through the metal center which agree well with the theoretical calculations. We are currently extending these promising synthetic routes in the search for a new series of rigid-rod multimetallic assemblies of nanosized dimensions.

Table 2
Selected bond lengths (Å) and angles (°) for complex **1**

Fe(1)–Cp	1.6504
Fe(1)–C_5H_4	1.6470
C(17)–C(18)	1.174(3)
C(14)–C(17)–C(18)	178.8(2)
Dihedral angles (°) between planes	
A and B	0.2
A and C	38.2
B and C	38.0

Planes: A, C(1)–C(2)–C(3)–C(4)–C(5); B, C(6)–C(7)–C(8)–C(9)–C(10); C, C(11)–C(12)–C(13)–C(14)–C(15)–C(16).

4. Experimental

4.1. General procedures

All reactions were carried out under N_2 with the use of standard inert atmosphere and Schlenk techniques, but no special precautions were taken to exclude oxygen during work-up. Solvents were pre-dried and distilled from appropriate drying agents. All chemicals, unless otherwise stated, were obtained from commercial sources and used as received. Preparative TLC was performed on 0.7 mm silica plates (Merck Kieselgel 60 GF_{254}) prepared in our laboratory. The starting compounds 4-ethynylphenylferrocene [14], *trans*-[$Pt(PEt_3)_2(Ph)Cl$] [15], *trans*-[$Pt(PBu_3)_2Cl_2$] [16] and *cis*-[$M(dppm)_2Cl_2$] (M = Ru, Os) [17] were prepared by reported procedures. Infrared spectra were recorded as CH_2Cl_2 solutions in a CaF_2 cell (0.5 mm path length) on a Perkin–Elmer Paragon 1000 PC or Nicolet Magna 550 Series II FTIR spectrometer. Proton NMR spectra were measured in $CDCl_3$ on a Jeol EX270 or a Varian INOVA 400 MHz FT NMR spectrometer. Chemical shifts were quoted relative to $SiMe_4$ ($\delta = 0$ ppm). FABMS were recorded on a Finnigan MAT SSQ710 mass spectrometer. Electronic absorption spectra were obtained with a Hewlett Packard 8453 UV–Vis spectrometer and steady-state visible luminescence spectra on a Photon Technology International (PTI) Alphascan spectrofluorimeter. Cyclic voltammetry experiments were done with a Princeton Applied Research (PAR) model 273A potentiostat, connected to an interfaced

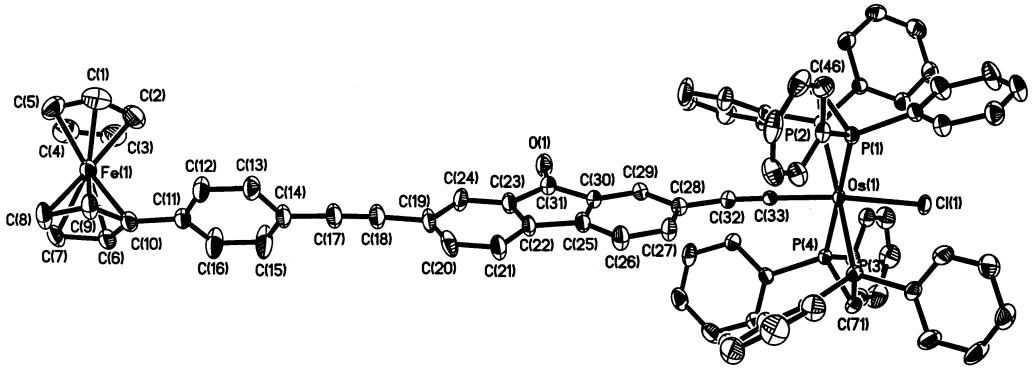

Fig. 6. A perspective view of **8**, showing the atomic labelling scheme. Thermal ellipsoids were drawn at the 25% probability level and hydrogen atoms are omitted for clarity.

Table 3
Selected bond lengths (Å) and angles (°) for complex **2a**

Fe(1)–Cp	1.6443
Fe(1)–C_5H_4	1.6430
C(17)–C(18)	1.188(4)
Br(1)–C(25)	1.892(3)
C(14)–C(17)–C(18)	176.7(3)
C(17)–C(18)–C(19)	177.6(3)
Dihedral angles (°) between planes	
A and B	2.5
A and C	7.7
A and D	8.3
B and C	8.0
B and D	7.1
C and D	4.9

Planes: A, C(1)–C(2)–C(3)–C(4)–C(5); B, C(6)–C(7)–C(8)–C(9)–C(10); C, C(11)–C(12)–C(13)–C(29)–C(30)–C(31); D, C(19)–C(20)–C(21)–C(22)–C(23)–C(24)–C(25)–C(26)–C(27)–C(28)–C(29)–C(30)–C(31).

Table 4
Selected bond lengths (Å) and angles (°) for complex **2c**

Fe(1)–Cp	1.6536
Fe(1)–C_5H_4	1.6452
C(17)–C(18)	1.184(8)
C(18)–C(18A)	1.391(14)
C(14)–C(17)–C(18)	178.8(7)
Dihedral angles (°) between planes	
A and B	1.8
A and C	9.8
B and C	10.1

Planes: A, C(1)–C(2)–C(3)–C(4)–C(5); B, C(6)–C(7)–C(8)–C(9)–C(10); C, C(11)–C(12)–C(13)–C(14)–C(15)–C(16).

Table 5
Selected bond lengths (Å) and angles (°) for complex **4**

Fe(1)–Cp	1.6517
Fe(1)–C_5H_4	1.6514
C(17)–C(18)	1.199(3)
C(32)–C(33)	1.161(4)
C(14)–C(17)–C(18)	177.2(3)
C(17)–C(18)–C(19)	178.9(3)
C(26)–C(32)–C(33)	178.8(3)
Dihedral angles (°) between planes	
A and B	3.3
A and C	7.6
A and D	7.6
B and C	7.6
B and D	6.3
C and D	3.1

Planes: A, C(1)–C(2)–C(3)–C(4)–C(5); B, C(6)–C(7)–C(8)–C(9)–C(10); C, C(11)–C(12)–C(13)–C(14)–C(15)–C(16); D, C(19)–C(20)–C(21)–C(22)–C(23)–C(24)–C(25)–C(26)–C(27)–C(28)–C(29)–C(30)–C(31).

Table 6
Selected bond lengths (Å) and angles (°) for complex **6**

Fe(1)–Cp	1.6477
Fe(1)–C_5H_4	1.6283
Fe(2)–Cp	1.6564
Fe(2)–C_5H_4	1.6371
C(17)–C(18)	1.180(10)
C(32)–C(33)	1.206(11)
Pt(1)–C(33)	1.990(8)
Pt(1)–P(1)	2.281(3)
Pt(1)–P(2)	2.272(3)
Pt(1)–C(58)	2.002(6)
C(58)–C(59)	1.194(8)
C(73)–C(74)	1.190(8)
C(14)–C(17)–C(18)	179.1(10)
C(17)–C(18)–C(19)	173.7(9)
C(29)–C(32)–C(33)	174.8(11)
Pt(1)–C(33)–C(32)	174.8(8)
P(1)–Pt(1)–P(2)	173.06(8)
Pt(1)–C(58)–C(59)	176.7(6)
C(58)–C(59)–C(60)	175.9(8)
C(70)–C(73)–C(74)	176.6(8)
C(73)–C(74)–C(75)	177.4(8)
Dihedral angles (°) between planes	
A and B	0.7
A and C	14.9
A and D	9.5
B and C	14.5
B and D	8.9
C and D	16.5
D and E	80.8
E and F	2.9
E and G	10.7
E and H	13.2
F and G	11.3
F and H	14.0
G and H	2.7

Planes: A, C(1)–C(2)–C(3)–C(4)–C(5); B, C(6)–C(7)–C(8)–C(9)–C(10); C, C(11)–C(12)–C(13)–C(14)–C(15)–C(16); D, C(19)–C(20)–C(21)–C(22)–C(23)–C(24)–C(25)–C(26)–C(27)–C(28)–C(29)–C(30)–C(31); E, C(60)–C(61)–C(62)–C(63)–C(64)–C(65)–C(66)–C(67)–C(68)–C(69)–C(70)–C(71)–C(72); F, C(75)–C(76)–C(77)–C(78)–C(79)–C(80); G, C(81)–C(82)–C(83)–C(84)–C(85); H, C(86)–C(87)–C(88)–C(89)–C(90).

computer employing PAR 270 electrochemical software. A conventional three-electrode configuration consisting of a glassy-carbon working electrode, a Pt-wire counter-electrode and a $Ag/AgNO_3$ reference electrode (0.1 M in acetonitrile) was used. The solvent in all measurements was deoxygenated CH_2Cl_2 and the supporting electrolyte was 0.1 M $[Bu_4N]PF_6$. Ferrocene was added as an internal standard at the end of each experiment and all potential data reported (vs. $Ag/AgNO_3$) were checked against the ferrocene–ferrocenium couple. The number of electrons transferred for each compound was estimated by comparing the peak height of the respective ferrocene oxidation wave with an equal concentration of the ferrocene standard added in the same system, in which one-electron oxidation was assumed. For DFT calculations at the B3LYP level, the basis set used for C and H atoms was 6-31G [18] while effective core

Table 7
Selected bond lengths (Å) and angles (°) for complex **8**

Fe(1)–Cp	1.6456
Fe(1)–C_5H_4	1.6352
C(17)–C(18)	1.199(8)
C(32)–C(33)	1.207(6)
Os(1)–C(33)	1.989(4)
Os(1)–Cl(1)	2.4895(13)
Os(1)–P(1)	2.3311(16)
Os(1)–P(2)	2.3711(15)
Os(1)–P(3)	2.3602(15)
Os(1)–P(4)	2.3487(16)
C(14)–C(17)–C(18)	178.5(8)
C(17)–C(18)–C(19)	176.6(8)
C(28)–C(32)–C(33)	173.7(5)
Os(1)–C(33)–C(32)	178.6(4)
Cl(1)–Os(1)–C(33)	174.38(13)
P(1)–Os(1)–P(2)	71.52(5)
P(1)–C(46)–P(2)	95.9(2)
P(3)–Os(1)–P(4)	71.16(5)
P(3)–C(71)–P(4)	95.9(2)
Dihedral angles (°) between planes	
A and B	2.6
A and C	14.5
A and D	53.9
B and C	16.6
B and D	52.0
C and D	68.3

Planes: A, C(1)–C(2)–C(3)–C(4)–C(5); B, C(6)–C(7)–C(8)–C(9)–C(10); C, C(11)–C(12)–C(13)–C(14)–C(15)–C(16); D, C(19)–C(20)–C(21)–C(22)–C(23)–C(24)–C(25)–C(26)–C(27)–C(28)–C(29)–C(30)–C(31).

potentials with a LanL2DZ basis set [19] were employed for Br, Cl, Fe, Os and P atoms. Polarization functions were added for Br ($\zeta_d = 0.389$), Cl ($\zeta_d = 0.514$) and P ($\zeta_d = 0.340$). For simplicity, PBu_3 was modeled by PMe_3 and the phenyl groups of the dppm were replaced by H atoms in the calculations.

4.2. Preparations of complexes

4.2.1. Synthesis of [(η^5-C_5H_5)Fe(η^5-C_5H_4)$C_6H_4C{\equiv}CRBr$] (**2a**), [(η^5-C_5H_5)Fe(η^5-C_5H_4)$C_6H_4C{\equiv}CRC{\equiv}CC_6H_4$($\eta^5$-$C_5H_4$)Fe($\eta^5$-$C_5H_5$)] (**2b**) and [($\eta^5$-$C_5H_5$)Fe($\eta^5$-$C_5H_4$)$C_6H_4C{\equiv}CC{\equiv}CC_6H_4$($\eta^5$-$C_5H_4$)Fe($\eta^5$-$C_5H_5$)] (**2c**) (R = *fluoren-9-one-2,7-diyl*)

2,7-Dibromofluoren-9-one (50 mg, 0.15 mmol) and 4-ethynylphenylferrocene (**1**, 42 mg, 0.15 mmol) in $^{i}Pr_2NH$–CH_2Cl_2 (30 cm^3, 1:1, v/v) were mixed under N_2 with catalytic amounts of $Pd(OAc)_2$ (1 mg), CuI (1 mg) and PPh_3 (2 mg). The mixture was refluxed for a period of 15 h, after which all volatile components were removed under reduced pressure. The residue was redissolved in CH_2Cl_2 and subsequently subjected to preparative TLC separation on silica using hexane–CH_2Cl_2 (3:2, v/v) as eluent. Three major orange bands were obtained from which the products were identified in descending order as **2c**, **2b** and **2a** ($R_f = 0.80$, 0.63 and 0.44, respectively) with respective yields of 10, 28 and 32%. **2a**—IR (CH_2Cl_2): 2213 ν(C≡C), 1723 ν(C=O) cm^{-1}. ^{1}H-NMR ($CDCl_3$): δ 4.05 (s, 5H, C_5H_5), 4.37 (t, 2H, $J_{H-H} = 1.9$ Hz, C_5H_4), 4.68 (t, 2H, $J_{H-H} = 1.9$ Hz, C_5H_4), 7.41 (d, 1H, $J_{H-H} = 7.8$ Hz, fluorenone), 7.45 (m, 4H, C_6H_4), 7.50 (d, 1H, $J_{H-H} = 7.8$ Hz, fluorenone), 7.62–7.68 (m, 2H, fluorenone) and 7.78–7.81 (m, 2H, fluorenone) ppm. FABMS: *m/z* 544 [M^+]. Anal. Found: C, 68.44; H, 3.29. Calc. for $C_{31}H_{19}BrFeO$: C, 68.54; H, 3.53%. **2b**—IR (CH_2Cl_2): 2213 ν(C≡C), 1721 ν(C=O) cm^{-1}. ^{1}H-NMR ($CDCl_3$): δ 4.18 (s, 10H, C_5H_5), 4.48 (m, 4H, C_5H_4), 4.80 (m, 4H, C_5H_4) and 7.26–7.80 (m, 14H, fluorenone + C_6H_4) ppm. FABMS: *m/z* 748 [M^+]. Anal. Found: C, 78.48; H, 4.29. Calc. for $C_{49}H_{32}Fe_2O$: C, 78.63; H, 4.31%. **2c**—IR (CH_2Cl_2): 2147 ν(C≡C) cm^{-1}. ^{1}H-NMR ($CDCl_3$): δ 4.07 (m, 10H, C_5H_5), 4.34 (m, 4H, C_5H_4), 4.68 (m, 4H, C_5H_4) and

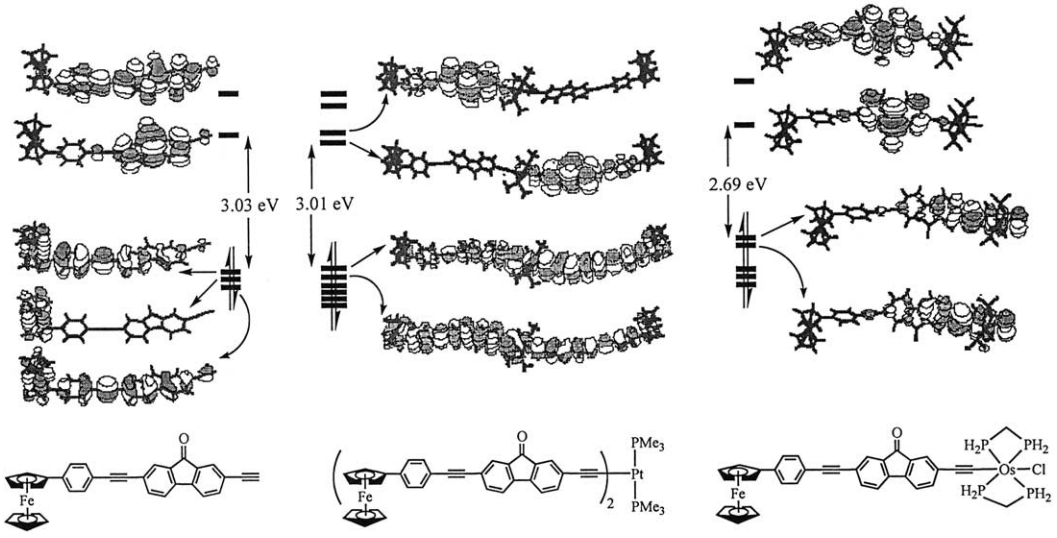

Fig. 7. Contour plots of the highest occupied (HOMO) and the lowest unoccupied molecular orbitals (LUMO) for **4**, **6** and **8**. In the calculations, the PBu_3 ligands were modeled by PMe_3 groups whereas the phenyl rings of dppm were modeled by H atoms.

7.43–7.55 (m, 8H, C_6H_4) ppm. FABMS: *m/z* 570 [M^+]. Anal. Found: C, 75.58; H, 4.50. Calc. for $C_{36}H_{26}Fe_2$: C, 75.82; H, 4.60%.

4.2.2. Synthesis of [(η^5-C_5H_5)Fe(η^5-C_5H_4)C_6H_4C≡CRC≡CSiMe$_3$] (R = fluoren-9-one-2,7-diyl) (3)

A mixture of **2a** (54 mg, 0.10 mmol), $Me_3SiC{\equiv}CH$ (20 mg, 0.20 mmol) and freshly distilled $^iPr_2NH$ (15 cm^3) combined with catalytic quantities of $Pd(OAc)_2$ (1.5 mg), CuI (1.5 mg) and PPh_3 (3 mg) in CH_2Cl_2 (15 cm^3) were allowed to reflux for 17 h. The red residue obtained by removing the volatile components in vacuo was redissolved in CH_2Cl_2. Upon filtration through a short silica pad, the filtrate was concentrated and purified by preparative TLC ($R_f = 0.38$) using hexane–CH_2Cl_2 (4:1, v/v) as eluent to yield **3** as an orange-red solid (51 mg, 91%). IR (CH_2Cl_2): 2204, 2157 ν(C≡C), 1721 ν(C=O) cm^{-1}. ^{1}H-NMR ($CDCl_3$): δ 0.27 (s, 9H, Me), 4.05 (s, 5H, C_5H_5), 4.37 (t, 2H, $J_{H-H} = 2.0$ Hz, C_5H_4), 4.68 (t, 2H, $J_{H-H} = 2.0$ Hz, C_5H_4), 7.46 (m, 4H, C_6H_4), 7.48 (d, 1H, $J_{H-H} = 8.0$ Hz, fluorenone), 7.51 (d, 1H, $J_{H-H} = 8.0$ Hz, fluorenone), 7.60 (dd, 1H, $J_{H-H} = 1.6$, 8.0 Hz, fluorenone), 7.66 (dd, 1H, $J_{H-H} = 1.6$, 8.0 Hz, fluorenone), 7.76 (m, 1H, fluorenone) and 7.81 (m, 1H, fluorenone) ppm. FABMS: *m/z* 560 [M^+]. Anal. Found: C, 77.01; H, 4.89. Calc. for $C_{36}H_{28}FeOSi$: C, 77.14; H, 5.03%.

4.2.3. Synthesis of [(η^5-C_5H_5)Fe(η^5-C_5H_4)C_6H_4C≡CRC≡CH] (R = fluoren-9-one-2,7-diyl) (4)

To a solution of **3** (28 mg, 0.05 mmol) in Et_2O (10 cm^3) was added K_2CO_3 (7 mg, 0.05 mmol) in MeOH (15 cm^3). The mixture was stirred for 24 h at room temperature (r.t.). After evaporation of the solvent, the crude product was dissolved in CH_2Cl_2 and chromatographed on silica plates ($R_f = 0.33$) eluting with hexane–CH_2Cl_2 (3:2, v/v) to afford pure **4** as an orange powder in 82% yield (20 mg). IR (CH_2Cl_2): 3302 ν(≡CH), 2204, 2104 ν(C≡C), 1721 ν(C=O) cm^{-1}. ^{1}H-NMR ($CDCl_3$): δ 3.19 (s, 1H, C≡CH), 4.05 (s, 5H, C_5H_5), 4.37 (t, 2H, $J_{H-H} = 2.0$ Hz, C_5H_4), 4.68 (t, 2H, $J_{H-H} = 2.0$ Hz, C_5H_4), 7.46 (m, 4H, C_6H_4), 7.49–7.55 (m, 2H, fluorenone), 7.64 (dd, 1H, $J_{H-H} = 1.6$, 8.0 Hz, fluorenone), 7.67 (dd, 1H, $J_{H-H} = 1.6$, 8.0 Hz, fluorenone), 7.78 (m, 1H, fluorenone) and 7.82 (m, 1H, fluorenone) ppm. FABMS: *m/z* 488 [M^+]. Anal. Found: C, 81.02; H, 4.05. Calc. for $C_{33}H_{20}FeO$: C, 81.16; H, 4.13%.

4.2.4. Synthesis of trans-[(η^5-C_5H_5)Fe(η^5-C_5H_4)C_6H_4C≡CRC≡CPt(PEt_3)$_2$Ph] (R = fluoren-9-one-2,7-diyl) (5)

Compound **4** (15 mg, 0.03 mmol) and *trans*-[Pt(PEt_3)$_2$(Ph)Cl] (17 mg, 0.03 mmol) were dissolved in $^iPr_2NH$ (15 cm^3) and CH_2Cl_2 (10 cm^3). After the addition of CuI (2 mg), the red solution was stirred at r.t. over 18 h. Concentration of the solution and subsequent purification by silica TLC ($R_f = 0.44$) using hexane–CH_2Cl_2 (3:2, v/v) as eluent readily led to the isolation of the title compound **5** as a red crystalline solid in 53% yield (16 mg). IR (CH_2Cl_2): 2209, 2089 ν(C≡C), 1717 ν(C=O) cm^{-1}. ^{1}H-NMR ($CDCl_3$): δ 1.05–1.14 (m, 18H, CH_3), 1.72–1.79 (m, 12H, CH_2), 4.05 (s, 5H, C_5H_5), 4.36 (t, 2H, $J_{H-H} = 1.8$ Hz, C_5H_4), 4.68 (t, 2H, $J_{H-H} = 1.8$ Hz, C_5H_4), 6.81 (t, 1H, $J_{H-H} = 8.1$ Hz, H_{para} of Ph), 6.97 (t, 2H, $J_{H-H} = 8.1$ Hz, H_{meta} of Ph), 7.31–7.51 (m, 9H, fluorenone + C_6H_4 + H_{ortho} of Ph), 7.56–7.62 (m, 2H, fluorenone) and 7.77 (m, 1H, fluorenone) ppm. ^{31}P{^{1}H}-NMR ($CDCl_3$): δ 11.12 ($^1J_{Pt-P} = 2630$ Hz) ppm. FABMS: *m/z* 996 [M^+]. Anal. Found: C, 61.30; H, 5.25. Calc. for $C_{51}H_{54}FeOP_2Pt$: C, 61.51; H, 5.47%.

4.2.5. Synthesis of trans-[(η^5-C_5H_5)Fe(η^5-C_5H_4)C_6H_4C≡CRC≡CPt(PBu_3)$_2$C≡CRC≡CC_6H_4(η^5-C_5H_4)Fe(η^5-C_5H_5)] (R = fluoren-9-one-2,7-diyl) (6)

The compound *trans*-[Pt(PBu_3)$_2$$Cl_2$] (20 mg, 0.03 mmol) and two molar equivalents of **4** (29 mg, 0.06 mmol) were stirred in a mixture of $^iPr_2NH$–CH_2Cl_2 (30 cm^3, 1:1, v/v) at r.t. in the presence of CuI (1.5 mg). Stirring was continued for 18 h and evaporation of the volatile components left behind a reddish residue, purification of which was accomplished by preparative TLC eluting with hexane–CH_2Cl_2 (3:2, v/v). From the red band ($R_f = 0.30$) was obtained product **6** and a pure sample of it was isolated in 46% (43 mg) after recrystallization from a hexane–CH_2Cl_2 mixture. IR (CH_2Cl_2): 2213, 2093 ν(C≡C), 1718 ν(C=O) cm^{-1}. ^{1}H-NMR ($CDCl_3$): δ 0.93–0.96 (m, 18H, CH_3), 1.42–1.51 (m, 12H, CH_2CH_3), 1.59 (m, 12H, PCH_2CH_2), 2.12–2.14 (m, 12H, PCH_2), 4.05 (s, 10H, C_5H_5), 4.36 (t, 4H, $J_{H-H} = 2.0$ Hz, C_5H_4), 4.68 (t, 4H, $J_{H-H} = 2.0$ Hz, C_5H_4), 7.38 (m, 4H, fluorenone), 7.43–7.46 (m, 10H, fluorenone + C_6H_4), 7.55 (m, 2H, fluorenone), 7.61–7.63 (m, 2H, fluorenone) and 7.77 (m, 2H, fluorenone) ppm. ^{31}P{^{1}H}-NMR ($CDCl_3$): δ 4.40 ($^1J_{Pt-P} = 2368$ Hz). FABMS: *m/z* 1574 [M^+]. Anal. Found: C, 68.53; H, 5.70. Calc. for $C_{90}H_{92}Fe_2O_2P_2Pt$: C, 68.66; H, 5.89%.

4.2.6. Synthesis of trans-[(η^5-C_5H_5)Fe(η^5-C_5H_4)C_6H_4C≡CRC≡CRu(dppm)$_2$Cl] (R = fluoren-9-one-2,7-diyl) (7)

A mixture of **4** (24 mg, 0.05 mmol), *cis*-[Ru(dppm)$_2$$Cl_2$] (47 mg, 0.05 mmol) and $NaPF_6$ (17 mg, 0.10 mmol) in CH_2Cl_2 (20 cm^3) were stirred for 4 h at r.t. The resulting red solution was filtered through a short pad of Celite to remove any excess $NaPF_6$ and NaCl byproduct, and DBU (7.6 mg, 0.05 mmol) was then added. After stirring for 2 h, the solvent was removed in vacuo and the solid was washed with diethyl ether (20 cm^3). The residue was redissolved in CH_2Cl_2 and filtration through a short alumina column using pure CH_2Cl_2 as eluent afforded the title complex as a

Table 8
Summary of crystal structure data for complexes **1**, **2a**, **2c**, **4**, **6** and **8**

	1	**2a**	**2c**	**4**	**6**	**8**·2CH_2Cl_2·CH_3OH
Empirical formula	$C_{18}H_{14}Fe$	$C_{31}H_{19}BrFeO$	$C_{36}H_{26}Fe_2$	$C_{33}H_{20}FeO$	$C_{90}H_{92}Fe_2O_2P_2Pt$	$C_{86}H_{71}Cl_5FeO_2OsP_4$
Molecular weight	286.14	543.22	570.27	488.34	1574.37	1683.61
Crystal size (mm^3)	0.28 × 0.17 × 0.10	0.29 × 0.20 × 0.14	0.34 × 0.09 × 0.07	0.35 × 0.33 × 0.18	0.30 × 0.22 × 0.12	0.31 × 0.19 × 0.15
Crystal system	orthorhombic	monoclinic	monoclinic	monoclinic	triclinic	triclinic
Space group	$P2_12_12_1$	$P2_1/n$	$P2_1/n$	$P2_1/n$	$P\bar{1}$	$P\bar{1}$
Unit cell dimensions						
a (Å)	9.8097(5)	10.4702(8)	7.887(2)	10.3811(10)	10.8831(11)	11.465(5)
b (Å)	10.7905(6)	19.6271(14)	16.013(5)	19.817(2)	13.2049(14)	11.465(5)
c (Å)	12.7294(7)	12.3843(9)	10.629(3)	12.4389(13)	28.812(3)	30.058(13)
α (°)					90.289(2)	92.271(5)
β (°)		114.6180(10)	102.399(5)	113.262(2)	97.798(2)	92.271(5)
γ (°)					110.819(2)	107.46(8)
U ($Å^3$)	1347.43(13)	2313.6(3)	1311.1(7)	2350.9(4)	3828.1(7)	3761(3)
D_{calc} (g cm^{-3})	1.411	1.560	1.444	1.380	1.366	1.487
Z	4	4	2	4	2	2
μ(Mo–K_α) (mm^{-1})	1.100	2.402	1.130	0.666	2.286	2.192
F(0 0 0)	592	1096	588	1008	1616	1700
θ range (°)	2.47–27.51	2.08–27.54	2.34–24.99	2.06–27.50	1.43–25.00	1.86–28.41
Reflections collected	7861	13 582	5943	13 826	19 144	22 406
Unique reflections	3023	5114	2225	5315	13 211	16 491
R_{int}	0.0179	0.0307	0.0690	0.0321	0.0476	0.0389
Observed reflections [$I > 2\sigma(I)$]	2843	3266	1342	3403	5911	11 062
No. of parameters	229	307	172	397	874	892
R_1, wR_2 [$I > 2\sigma(I)$]	0.0234, 0.0642	0.0354, 0.0824	0.0736, 0.1775	0.0370, 0.0889	0.0650, 0.1489	0.0433, 0.0958
R_1, wR_2 (all data)	0.0252, 0.0658	0.0653, 0.0921	0.1167, 0.2191	0.0688, 0.1017	0.1656, 0.1945	0.0770, 0.1075
Goodness-of-fit on F^2	1.040	0.940	0.849	0.930	0.930	0.800
Residual extrema in final diff. map (e $Å^{-3}$)	0.195 to −0.215	0.399 to −0.500	0.773 to −1.044	0.250 to −0.312	1.278 to −0.785	1.070 to −0.710

reddish-brown solid in 42% yield (29 mg) after recrystallization from an evaporated hexane–CH_2Cl_2 solution at r.t. IR (CH_2Cl_2): 2066 ν(C≡C), 1715 ν(C=O) cm^{-1}. ^{1}H-NMR ($CDCl_3$): δ 4.05 (s, 5H, C_5H_5), 4.36 (m, 2H, C_5H_4), 4.68 (m, 2H, C_5H_4), 4.93 (m, 4H, CH_2), 7.09–7.20 (m, 30H, fluorenone) and 7.27–7.46 (m, 20H, fluorenone) ppm. ^{31}P{^{1}H}-NMR ($CDCl_3$): δ −5.60 ppm. FABMS: m/z 1394 [M^+]. Anal. Found: C, 71.44; H, 4.38. Calc. for $C_{83}H_{63}ClFeOP_4Ru$: C, 71.58; H, 4.56%.

*4.2.7. Synthesis of trans-[(η^5-C_5H_5)Fe(η^5-C_5H_4)C_6H_4C≡CRC≡COs(dppm)$_2$Cl] (R = fluoren-9-one-2,7-diyl) (**8**)*

cis-[Os(dppm)$_2$$Cl_2$] (52 mg, 0.05 mmol) was added to a solution of **4** (24 mg, 0.05 mmol) in CH_2Cl_2 (20 cm^3) in the presence of $NaPF_6$ (17 mg, 0.10 mmol) and the mixture was stirred for 4 h. The resultant vinylidene solution was filtered and DBU (7.6 mg, 0.05 mmol) was added to give a deep green solution. After the solution was stirred for a further 2 h, the solvent was evaporated off and the residue was washed with diethyl ether (20 cm^3). The crude solid was then dissolved in CH_2Cl_2 and filtered through a short alumina column eluting with the same solvent. A greenish-red crystalline solid of **8** was collected in 53% yield (39 mg). IR (CH_2Cl_2): 2062 ν(C≡C), 1715 ν(C=O) cm^{-1}. ^{1}H-NMR ($CDCl_3$): δ 4.06 (s, 5H, C_5H_5), 4.36 (m, 2H, C_5H_4), 4.68 (m, 2H, C_5H_4), 5.48 (m, 4H, CH_2), 7.09–7.20 (m, 30H, fluorenone) and 7.27–7.46 (m, 20H, fluorenone) ppm. ^{31}P{^{1}H}-NMR ($CDCl_3$): δ −48.00 ppm. FABMS: m/z 1482 [M^+]. Anal. Found: C, 67.02; H, 3.99. Calc. for $C_{83}H_{63}ClFeOOsP_4$: C, 67.28; H, 4.29%.

5. Crystallography

Single crystals of **1**, **2a**, **2c**, **4**, **6** and **8** suitable for X-ray crystallographic analyses were chosen and mounted on a glass fiber using epoxy resin. Crystal data and other experimental details are summarized in Table 8. The diffraction experiments were carried out at r.t. on a Bruker Axs SMART 1000 CCD area-detector diffractometer using graphite-monochromated Mo–K_α radiation ($\lambda = 0.71073$ Å). At the end of data collection, no crystal decay was observed. The collected frames were processed with the software SAINT [20a] and an absorption correction (SADABS) was applied to the collected reflections [20b]. The structures were solved by direct methods (for **1**, **2a**, **2c** and **8**) and Patterson method (for **4** and **6**), and expanded by difference Fourier syntheses using the software SHELTXL [21]. Structure refinements

were made on F^2 by the full-matrix least-squares technique. In each case, all the non-hydrogen atoms were refined with anisotropic displacement parameters. The hydrogen atoms were placed in their ideal positions and not refined.

6. Supplementary material

Crystallographic data (comprising hydrogen atom coordinates, thermal parameters and full tables of bond lengths and angles) for the structural analysis have been deposited with the Cambridge Crystallographic Centre (Deposition Nos. 209514–209519). Copies of this information may be obtained free of charge from The Director, CCDC, 12 Union Road, Cambridge, CB2 1EZ, UK (Fax: +44-1223-336-033; e-mail: deposit@ccdc.cam.ac.uk or www: http://www.ccdc.cam.ac.uk).

Acknowledgements

Financial support from the Faculty Research Grants of Hong Kong Baptist University (FRG/00-01/II-57) is gratefully acknowledged.

References

[1] (a) P. Nguyen, P. Gómez-Elipe, I. Manners, Chem. Rev. 99 (1999) 1515;
(b) R.P. Kingsborough, T.M. Swager, Prog. Inorg. Chem. 48 (1999) 123;
(c) F. Paul, C. Lapinte, Coord. Chem. Rev. 178–180 (1998) 431;
(d) V.W.-W. Yam, Chem. Commun. (2001) 789;
(e) U.H.F. Bunz, Y. Rubin, Y. Tobe, Chem. Soc. Rev. 28 (1999) 107;
(f) A. Aviram (Ed.), Molecular Electronics: Science and Technology, Conference Proceedings No. 262, American Institute of Physics, New York, 1992;
(g) S. Barlow, D. O'Hare, Chem. Rev. 97 (1997) 637;
(h) F. Diederich, Chem. Commun. (2001) 219;
(i) F. Diederich, Y. Rubin, Angew. Chem. Int. Ed. Engl. 31 (1992) 1101.

[2] (a) R. Ziessel, M. Hissler, A. El-Ghayoury, A. Harriman, Coord. Chem. Rev. 178–180 (1998) 1251;
(b) V. Balzani, A. Juris, M. Venturi, S. Campagna, S. Serroni, Chem. Rev. 96 (1996) 759;
(c) S. Kawabata, I. Yamazaki, Y. Nishimura, Bull. Chem. Soc. Jpn. 70 (1997) 1125;
(d) J.A. McCleverty, M.D. Ward, Acc. Chem. Res. 31 (1998) 842;
(e) M.D. Ward, Chem. Soc. Rev. 24 (1995) 121;
(f) M. Malaun, R. Kowallick, A.M. McDonagh, M. Marcaccio, R.L. Paul, I. Asselberghs, K. Clays, A. Persoons, B. Bildstein, C. Fiorini, J.-M. Nunzi, M.D. Ward, J.A. McCleverty, J. Chem. Soc. Dalton Trans. (2001) 3025.

[3] A. Hradsky, B. Bildstein, N. Schuler, H. Schottenberger, P. Jaitner, K.-H. Ongania, K. Wurst, J.-P. Launay, Organometallics 16 (1997) 392.

[4] C. Le Vanda, D.O. Cowan, J. Am. Chem. Soc. 96 (1974) 6728.

[5] (a) K.R. Justin Thomas, J.T. Lin, K.-J. Lin, Organometallics 18 (1999) 5285;
(b) K.R. Justin Thomas, J.T. Lin, Y.S. Wen, Organometallics 19 (2000) 1008;
(c) W.-M. Xue, F.E. Kühn, E. Herdtweck, Q. Li, Eur. J. Inorg. Chem. (2001) 213.

[6] (a) R.D. Adams, O.-S. Kwon, B. Qu, M.D. Smith, Organometallics 20 (2001) 5225;
(b) R.D. Adams, B. Qu, M.D. Smith, T.A. Albright, Organometallics 21 (2002) 2970;
(c) R.D. Adams, B. Qu, M.D. Smith, Organometallics 21 (2002) 3867;
(d) R.D. Adams, B. Qu, M.D. Smith, Organometallics 21 (2002) 4847;
(e) N.J. Long, A.J. Martin, R. Vilar, A.J.P. White, D.J. Williams, M. Younus, Organometallics 18 (1999) 4261;
(f) M.C.B. Colbert, J. Lewis, N.J. Long, P.R. Raithby, A.J.P. White, D.J. Williams, J. Chem. Soc. Dalton Trans. (1997) 99;
(g) N.D. Jones, M.O. Wolf, D.M. Giaquinta, Organometallics 16 (1997) 1352;
(h) O. Lavastre, E. Even, P.H. Dixneuf, A. Pacreau, J.-P. Vairon, Organometallics 15 (1996) 1530;
(i) O. Lavastre, J. Plass, P. Bachmann, S. Guesmi, C. Moinet, P.H. Dixneuf, Organometallics 16 (1997) 184;
(j) N.J. Long, A.J. Martin, A.J.P. White, D.J. Williams, M. Fontani, F. Laschi, P. Zanello, J. Chem. Soc. Dalton Trans. (2000) 3387.

[7] (a) W.-Y. Wong, G.-L. Lu, K.-F. Ng, C.-K. Wong, K.-H. Choi, J. Organomet. Chem. 637–639 (2001) 159;
(b) W.-Y. Wong, G.-L. Lu, K.-F. Ng, K.-H. Choi, Z. Lin, J. Chem. Soc. Dalton Trans. (2001) 3250;
(c) W.-Y. Wong, K.-Y. Ho, K.-H. Choi, J. Organomet. Chem. 670 (2003) 17.

[8] (a) D. Neher, Macromol. Rapid Commun. 22 (2001) 1365;
(b) R.D. McCullough, Adv. Mater. 10 (1998) 93;
(c) J. Lewis, P.R. Raithby, W.-Y. Wong, J. Organomet. Chem. 556 (1998) 219;
(d) W.-Y. Wong, W.-K. Wong, P.R. Raithby, J. Chem. Soc. Dalton Trans. (1998) 2761.;
(e) W.-Y. Wong, K.-H. Choi, G.-L. Lu, J.-X. Shi, Macromol. Rapid Commun. 22 (2001) 461;
(f) W.-Y. Wong, G.-L. Lu, K.-H. Choi, J.-X. Shi, Macromolecules 35 (2002) 3506;
(g) W.-Y. Wong, K.-H. Choi, G.-L. Lu, J.-X. Shi, P.-Y. Lai, S.-M. Chan, Z. Lin, Organometallics 20 (2001) 5446;
(h) W.-Y. Wong, K.-H. Choi, G.-L. Lu, Z. Lin, Organometallics 21 (2002) 4475.

[9] (a) M.C.B. Colbert, S.L. Ingham, J. Lewis, N.J. Long, P.R. Raithby, J. Chem. Soc. Dalton Trans. (1994) 2215;
(b) D. Touchard, P. Haquette, N. Pirio, L. Toupet, P.H. Dixneuf, Organometallics 12 (1993) 3132;
(c) A.J. Hodge, S.L. Ingham, A.K. Kakkar, M.S. Khan, J. Lewis, N.J. Long, D.G. Parker, P.R. Raithby, J. Organomet. Chem. 488 (1995) 205;
(d) M.C.B. Colbert, J. Lewis, N.J. Long, P.R. Raithby, M. Younus, A.J.P. White, D.J. Williams, N.N. Payne, L. Yellowlees, D. Beljonne, N. Chawdhury, R.H. Friend, Organometallics 17 (1998) 3034;
(e) W.-Y. Wong, C.-K. Wong, G.-L. Lu, J. Organomet. Chem. 671 (2003) 27.

[10] (a) D. Osella, L. Milone, C. Nervi, M. Ravera, J. Organomet. Chem. 488 (1995) 1;
(b) D. Osella, R. Gobetto, C. Nervi, M. Ravera, R. D'Amato, M.V. Russo, Inorg. Chem. Commun. 1 (1998) 239;
(c) H. Fink, N.J. Long, A.J. Martin, G. Opromolla, A.J.P. White, D.J. Williams, P. Zanello, Organometallics 16 (1997) 2646.

[11] J.-G. Rodriguez, A. Oñate, R.M. Martin-Villamil, I. Fonseca, J. Organomet. Chem. 513 (1996) 71.
[12] (a) A.D. Becke, J. Chem. Phys. 98 (1993) 5648;
(b) B. Miehlich, A. Savin, H. Stoll, H. Preuss, Chem. Phys. Lett. 157 (1989) 200;
(c) C. Lee, W. Yang, G. Parr, Phys. Rev. B 37 (1988) 785.
[13] G. Schaftenaar, Molden ver. 3.5, CAOS/CAMM Center Nijmegen, Toernooiveld, Nijmegen, The Netherlands, 1999.
[14] C. Simionescu, T. Lixandru, I. Mazilu, L. Tataru, J. Organomet. Chem. 113 (1976) 23.
[15] J. Chatt, B.L. Shaw, J. Chem. Soc. (1960) 4020.
[16] G.B. Kauffman, L.A. Teter, Inorg. Synth. 7 (1963) 245.
[17] B.P. Sullivan, T.J. Meyer, Inorg. Chem. 21 (1982) 1037.
[18] P.C. Hariharan, J.A. Pople, Theor. Chim. Acta 28 (1973) 213.
[19] P.J. Hay, W.R. Wadt, J. Chem. Phys. 82 (1985) 299.
[20] (a) SAINT, Reference Manual, Siemens Energy and Automation, Madison, WI, 1994–1996;
(b) G.M. Sheldrick, SADABS, Empirical Absorption Correction Program, University of Göttingen, 1997.
[21] G.M. Sheldrick, SHELXTL™, Reference Manual, ver. 5.1, Madison, WI, 1997.